# Lamellar Structured Nanoparticles Formed by Complexes of a Cationic Block Copolymer and Perfluorodecanoic Acid

**André Laschewsky,*,†,‡ Murat Mertoglu,† Stefan Kubowicz,‡,§ and Andreas F. Thünemann*,⊥**

*Institute of Chemistry, University of Potsdam, Karl-Liebknecht-Strasse 24-25, 14476 Potsdam-Golm, Germany, Fraunhofer Institute of Applied Polymer Research IAP, Geiselbergstrasse 69, 14476 Potsdam-Golm, Germany, Max Planck Institute of Colloids and Interfaces, Am Mühlenberg 1, 14476 Golm, Germany, and Federal Institute for Materials Research and Testing, Richard-Willstaetter-Strasse 11, 12489 Berlin, Germany*

*Received July 13, 2006; Revised Manuscript Received October 23, 2006*

ABSTRACT: A double hydrophilic block copolymer was synthesized by controlled free radical polymerization, namely by the RAFT method, from a poly(ethylene oxide) macromonomer and a cationic acrylate. Stoichiometric complexes with sodium decanoate and with sodium perfluorodecanoate were prepared by self-assembly. Both complexes are soluble in water forming core−shell nanoparticles with hydrodynamic radii of 54 and 22 nm, respectively, and neutral $\zeta$ potentials. The complex containing decanoate decomposed upon dilution, while the complex with perfluorodecanoate is stable even against dialysis and in salt solution. Only the nanoparticles containing perfluorodecanoate show a strong contrast in small-angle X-ray scattering (SAXS). It is produced from their cores that have an elliptical shape (short axes = 8.5 nm, long axis = 23.3 nm) and a sharp density transition to the shell. The cores exhibit an internal lamellar structure with a long period of 3.65 nm consisting of fluorocarbon rich lamellae ($d_1$ = 3.00 nm) and lamellae enriched in ionic groups ($d_2$ = 0.65 nm). These fluorinated nanoparticles coexist in physiological buffer with human serum albumin and fibrinogen without inducing aggregation. Moreover, the content of α-helix of these serum proteins increased when in solution with the fluorinated nanoparticles.

## Introduction

The complexation of ionic surfactants with oppositely charged polyelectrolytes has been known for a long time.[1] By virtue of the possible versatile variations of the two reaction partners, a wealth of supramolecular assemblies has been created over the years. Still, the stoichiometric pairing of the ionic groups of the surfactant and the polyelectrolyte results typically in water-insoluble complexes. In order to overcome this problem, two main strategies have emerged. In the classical approach, nonstoichiometric complexes are produced, using generally an excess number of charged groups on the polyelectrolyte. This results inevitably in charged supramolecular assemblies. More recently, a second approach was developed based on double hydrophilic block copolymers, in which one block is a polyelectrolyte while the other one is a nonionic water-soluble polymer.[2] The latter strategy enables the assembly of noncharged water-soluble supramolecular structures, as even the stoichiometric complex of the polyelectrolyte block with the ionic surfactant is solubilized by the second hydrophilic block.[3] This type of complex was termed block ionomer complex "BIC."[4] It can be considered as an amphiphilic block copolymer ("macrosurfactant") held together by secondary valences, namely ionic bonds, instead of by covalent bonds. In particular, BICs give rise to amphiphilic supramolecular macrosurfactants with a brushy hydrophobic block.

The described strategy was handicapped for long by the difficulties to synthesize the required double-hydrophilic charged block copolymers. Living anionic polymerization for instance, which is traditionally the method of choice to prepare well-defined block copolymers, is limited to a small pool of suited monomers. Also, it requires frequently the chemical protection of the desired ionic groups during synthesis. Moreover, the typically accessible polyelectrolyte blocks, such as poly((meth)-acrylic acid) and poly(vinylpyridine)s[5] are subject to protonation/deprotonation equilibria and hence are charged only in a limited pH-window. This situation has changed dramatically with the arrival of the methods of controlled free radical polymerization, which inherently are compatible with the presence of water and charged groups. Particularly useful in this context is the RAFT technique, which enables the convenient polymerization of permanently ionic monomers, even in aqueous solution.[6−8] Although the synthesis of block copolymers with a permanently charged block has been reported only occasionally so far, the potential of the method is obvious. Also, the RAFT technique was shown to be suited for the polymerization of macromonomers.[8−10]

Polymeric micelles which are prepared by using the selective solubility of polymer blocks are one of the thriving topics of supramolecular assembly due to fundamental interests as well as due to potential applications, e.g., for catalysis, for surface modification, or for use as pharmaceutical drug carriers.[11−20] Polymeric micelles in water can be prepared from amphiphilic copolymers bearing both hydrophilic and hydrophobic blocks, or as pointed out above, from complexes of double hydrophilic copolymers bearing one ionic block with oppositely charged surfactants. Importantly for uses in biological environments, such complexes should be noncharged to exhibit good biocompatibility. A preferred nonionic hydrophilic block for uses in

* Corresponding authors. Telephone: x-49331 5681327. Fax: x-49331 5683000. E-mail: (A.L.) laschewsky@iap.fhg.de; (A.F.T.) andreas.thuenemann@bam.de.
† Institute of Chemistry, University of Potsdam.
‡ Fraunhofer Institute of Applied Polymer Research IAP.
§ Max Planck Institute of Colloids and Interfaces.
⊥ Federal Institute for Materials Research and Testing.

10.1021/ma061573k CCC: $33.50 
Published on Web 12/08/2006

biological environments is poly(ethylene oxide) PEO. Mostly, linear PEO chains have been described so far in this context, but an interesting alternative are PEO brushes which are increasingly employed.[8,10,21−25]

In the context of biocompatible nanoparticles a coating of particles with poly(ethylene oxide)s is often used to avoid their uptake by the reticuloendothelial system. The covalent binding of PEO to molecules and particles is most often referred as PEGylation[26] (PEO and PEG are used as synonyms).

Being interested in nanoparticulate polymeric carriers for biomedical uses, we explored therefore the complexation of sodium alkanoates as model ionic surfactants with a cationic double hydrophilic block copolymer. The block copolymer is made by sequential aqueous RAFT polymerization of an acrylate bearing a fully quaternized ammonium group (**M1**) and a nonionic PEO macromonomer (**M2**). Sodium decanoate and sodium perfluorodecanoate were chosen as surfactants for complexation, in order to compare the influence of the nature of the hydrophobic chain. It has been shown earlier that polyampholytes with alternating cationic and anionic monomers can be complexed with dodecanoic acid and perfluorododecanoic acid via self-assembly and generate nanoparticles with sizes in the range of 3−5 nm (dressed micelles).[27] The nanoparticles of the polyampholyte perfluorododecanoic acid complex induced an α-helix-rich structure in the amyloid fibril forming B18 peptide. In contrast, the nanoparticles of the polyampholyte dodecanoic acid complex induced precipitation of B18.[28]

Here we present the initial step of a long-term project aimed at the understanding of the influence of BICs on the secondary structure of proteins and peptides. The supramolecular macrosurfactant structures **H−BIC** and **F−BIC** are shown in Figure 1. Because of the use of a macromonomer for the nonionic block, the macrosurfactant has a double-brush structure (Scheme 1). Such an architecture of polymeric amphiphiles has barely been described and studied.[22,29]

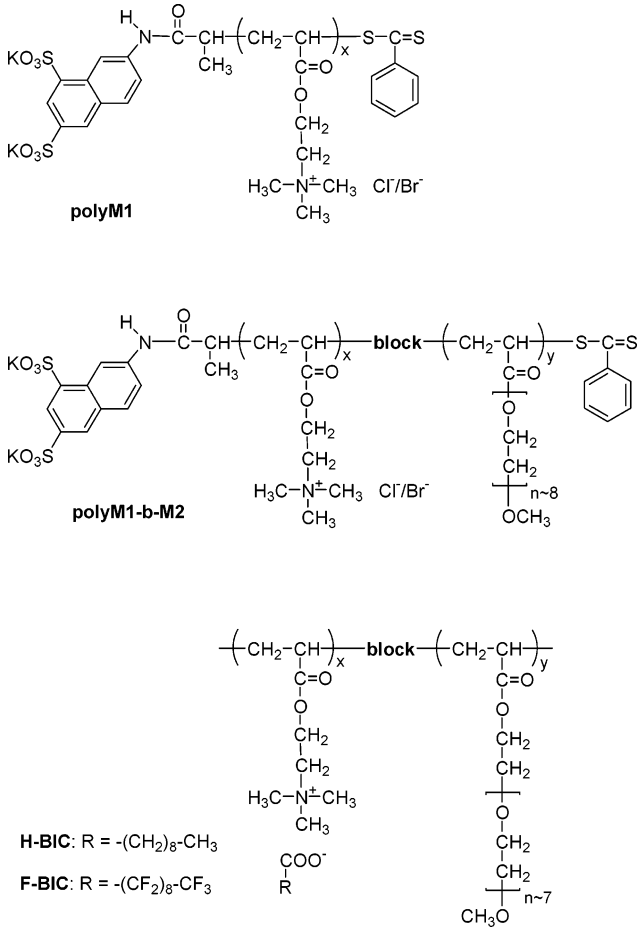


**Figure 1.** Structure of the macro RAFT agent **polyM1**, block copolymer **polyM1-*block*-M2**, and the alkylated complex (**H−BIC**) and the fluorinated complex (**F−BIC**).

**Scheme 1. Schematic Architecture of Amphiphilic Block Copolymers (Macrosurfactants)[a]**

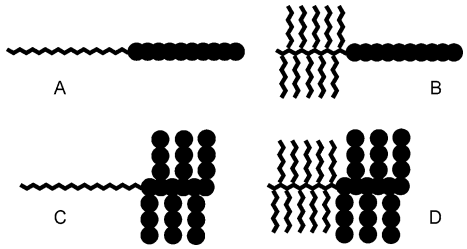


[a] All linear (A), brush type hydrophobic block (B), brush type hydrophilic block (C), and double brush type (D).

## Experimental Section

**Materials.** Decanoic acid (capric acid, 98%+, Fluka) and perfluorodecanoic acid (perfluorocapric acid, 97%+, Fluka) were used as received. Monomer 2-acryloyloxyethylammonium chloride (**M1**, $M_r$ = 193.67) was employed as 80% aqueous solution (Aldrich). Inhibitor 4-methoxyphenol was removed by extracting three times with diethyl ether prior to polymerization. Monomer poly(ethylene oxide)monomethyletheracrylate (**M2**, $M_r$ = 454, average degree of polymerization of PEO = 8.4, Aldrich) was purified from inhibitor 4-methoxyphenol by filtration over basic $Al_2O_3$ (activity I, 0.063−0.20 mesh, Merck). The synthesis of RAFT agent dipotassium 7-(2-thiobenzoylsulfanylpropionylimino)-naphthalene-1,3-disulfonate is described elsewhere.[8]

The chromophore labeled macro RAFT agent **poly-M1** is made by polymerization of 4.13 g of 80 wt % aqueous solution of **M1** (17.1 mmol) in 20 mL of 0.5 M aqueous NaBr at 55 °C for 3.5 h, using $1 \times 10^{-4}$ mol of 2,2′-azobis(2-methyl-*N*-phenylproprionamidine)dihydrochloride (**V-545**, $M_r$ = 423.39, Wako Pure Chemical Industries) as initiator and $4 \times 10^{-4}$ mol of dipotassium 7-(2-thiobenzoylsulfanyl propionylimino) naphthalene-1,3-disulfonate as RAFT agent. The polymer is purified by dialysis against water (Zellu Trans, Roth (Germany), nominal cut off molar mass 3500 g $mol^{-1}$). Yield: 2.9 g. According to elemental analysis, the polycation bears a mixture of $Cl^-$ (57%) and $Br^-$ (43%) as counter ions. Number-average molar mass $M_n = 1.0 \times 10^4$ g $mol^{-1}$ and polydispersity index ($M_w/M_n$) was 1.22 according to MALLS−SEC.

The dihydrophilic copolymer **polyM1-*block*-M2** was synthesized via RAFT polymerization of 3.8 g (8.4 mmol) of macromonomer **M2** in 25 mL of water at 55 °C for 6 h, using $3.2 \times 10^{-5}$ mol of 2,2′-azobis(2-methyl-proprionamidine)dihydrochloride (**V-50**, $M_r$ = 271.19, Wako Pure Chemical Industries) as initiator and 1.39 g ($1.16 \times 10^{-4}$ mol) of **polyM1** as macro RAFT agent. Yield: 3.45 g (90%). The block copolymer was purified by dialysis against water (Zellu Trans, Roth (Germany), nominal cut off molar mass 3500 g $mol^{-1}$). Number-average molar mass = $3.9 \times 10^4$ g $mol^{-1}$ and polydispersity index ($M_w/M_n$) was 1.45 according to MALLS−SEC.

Nanoparticles of **H−BIC** were prepared as follows: decanoic acid (0.23 g, 1.36 mmol) was dissolved in diethyl ether (15 mL), 0.1 M aqueous NaOH (13.6 mL) was added, and the biphasic system was stirred for 10 min. Then, it was added to a 60 °C hot solution of 1.00 g of copolymer **polyM1-*block*-M2** dissolved in 100 mL of water. The mixture was stirred vigorously for 6 h at 60 °C. Finally, the solutions were cooled to ambient temperature while stirring. Nanoparticles of **F−BIC** were prepared identically using nonadecafluorodecanoic acid (0.70 g, 1.36 mmol).

**Table 1. Composition and Molar Mass Data of the Synthesized Block Copolymer and Macro RAFT Agent**

| sample | amount of added block **M2** (wt %) | $M_n$ ($10^3$ g·mol$^{-1}$) | $DP_n$ of blocks |
|---|---|---|---|
| **polyM1** | | 10[a] | 52 |
| | | 9[b] | |
| | | 12[c] | |
| **polyM1-*block*-M2** | 75[e] | 39[a] | 66 |
| | 76[f] | 37[b] | |
| | | 80[c] | |
| | | 57[d] | |

[a] Determined by SEC-MALLS in 0.2 M aqueous $Na_2SO_4$ containing 1 wt % acetic acid. [b] Calculated via end group analysis of the naphthalene band at 251 nm. [c] Calculated via end group analysis of the C═S band at 485 nm. [d] Calculated via end group analysis of the mixed band at 301 nm. [e] Determined by $^1$H NMR. [f] Determined by microanalysis.

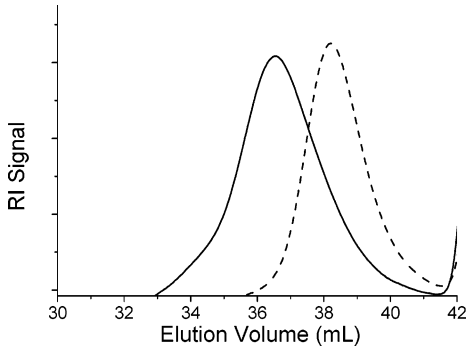


**Figure 2.** Aqueous SEC traces of the macro RAFT agent **polyM1** (dashed line) and **polyM1-block-M2** (solid line). Eluent 0.2 M aqueous $Na_2SO_4$ containing 1 wt % acetic acid.

HSA (albumin ≥96%, essential fatty acid free) and bovine plasma fibrinogen were purchased from Sigma and used without further purification. HSA has a molecular weight of $6.65 \times 10^4$ g mol$^{-1}$ and contains 585 amino acid residues. Fibrinogen has a molecular weight of $3.40 \times 10^5$ g mol$^{-1}$ and contains 2964 amino acid residues.

**Methods.** The analytical equipment and the experimental setup for NMR spectroscopy, UV−vis spectroscopy, and aqueous size exclusion chromatography equipped with a multiangle laser light scattering detector (MALLS−SEC) were described before.[8,10]

The dynamic light scattering measurements were carried out with a particle sizer, model HPPS 3.3-ET from Malvern Instruments, at a temperature of 25 °C. Zeta potential measurements were made with a Zeta Master S (Malvern Instruments, UK). The density of nanoparticles was determined with a vibrating tube densimeter model DMA 60/602 (Anton Paar, Graz, Austria).

The small-angle X-ray scattering measurements (SAXS) were performed with an Anton Paar HR−PHK pinhole camera, which was equipped with a xenon filled two-dimensional detector (512 × 512 pixel, $\Delta\theta \sim 0.02°$), at a temperature of 20 °C. The sample to detector distance was 610 mm. The scattering vector is defined in terms of the scattering angle $\theta$, and the wavelength $\lambda$ of the radiation (Cu K$\alpha$ = 0.154 nm) thus $s = 2/\lambda \sin(\theta/2)$ (note that $q = 2\pi s$). The SAXS measurements were repeated at the microfocus beamline at BESSY II (Berlin, Germany) to verify the results and to measure data of better statistics at high $s$ values. Dispersions of the particles with concentrations of 3 to 30 g L$^{-1}$ were transferred into glass capillaries with a diameter of 1 mm. The intensity measured was corrected by subtracting the intensity from a capillary filled with pure water.

Circular dichroism spectra were detected by a spectropolarimeter J715 from Jasco. The measurements were performed in the far-UV range (190−260 nm). CD was measured at pH 7.0 in $K_2HPO_4$/$KH_2PO_4$ buffer and the concentration of fibrinogen was 0.667 mM (0.5 g fibrinogen and 4.5 g L$^{-1}$ **F−BIC**).

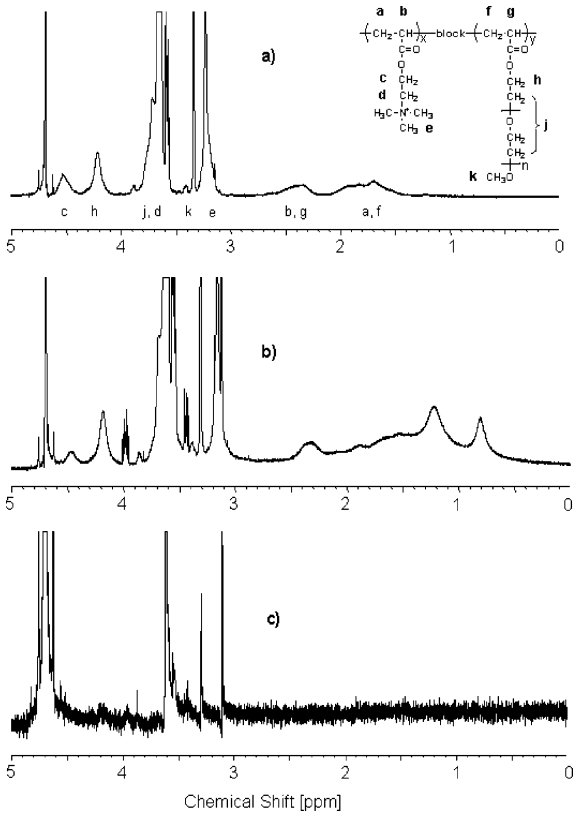


**Figure 3.** $^1$H NMR spectra of (from top to bottom): (a) block copolymer **polyM1-*block*-M2**, (b) its complex with sodium decanoate (**H−BIC**), and (c) its complex with perfluoro decanoate (**F−BIC**) in $D_2O$.

## Results and Discussion

**Block Copolymer Synthesis.** The preparation of block copolymers via RAFT is known to work smoothly if both blocks are based on monomers with the identical polymerizable moiety, or with polymerizable moieties of comparable reactivity.[30] Therefore, both blocks of the mixed cationic-nonionic double hydrophilic block copolymer **polyM1-*block*-M2** were based on acrylates.

Macro RAFT agent **polyM1** was synthesized in aqueous solution in the presence of RAFT agent dipotassium 7-(2-thiobenzoylsulfanylpropionylimino)naphthalene-1,3-disulfonate at 55 °C. The temperature was kept constant and the reaction time was limited to 3.5 h, since the RAFT agent is prone to hydrolysis at higher temperature for prolonged reaction times,[7,8,31] and the same risk exists for the active end groups of the propagating polymers chains. The particular RAFT agent was chosen as it was shown before to be well suited for controlling the polymerization of acrylates in aqueous solution, and the reinitiating "R" group bears a strong UV-chromophore (donor−acceptor substituted naphthalene moiety) that can be easily detected by UV-spectroscopy.[8] The reinitiating group is permanently fixed to the polymer chains, and makes the vast majority of the initiating end groups for the employed ratio of RAFT agent to initiator. Therefore, quantification of the absorbance of the naphthalene fragment at 251 nm (extinction coefficient $\epsilon$ = 47 100 L mol$^{-1}$ cm$^{-1}$) enables the efficient determination of the number-average molar mass $M_n$ of **polyM1** by end group analysis. Also, end group analysis is possible by analyzing the weak absorbance band of the C═S n−$\pi^*$ transition of the dithiobenzoate moiety in the visible ($\lambda_{max}$ = 483 nm in water, $\epsilon$ = 130 L mol$^{-1}$ cm$^{-1}$). The comparison of the results derived from both end groups allows a good

**Scheme 2. Preparation of Particles by Complexation of Cationic Block of Copolymer polyM1-*block*-M2 with the Ionic Surfactants Sodium Decanoate and Sodium Perfluorodecanoate, Named H−BIC and F−BIC, Respectively**

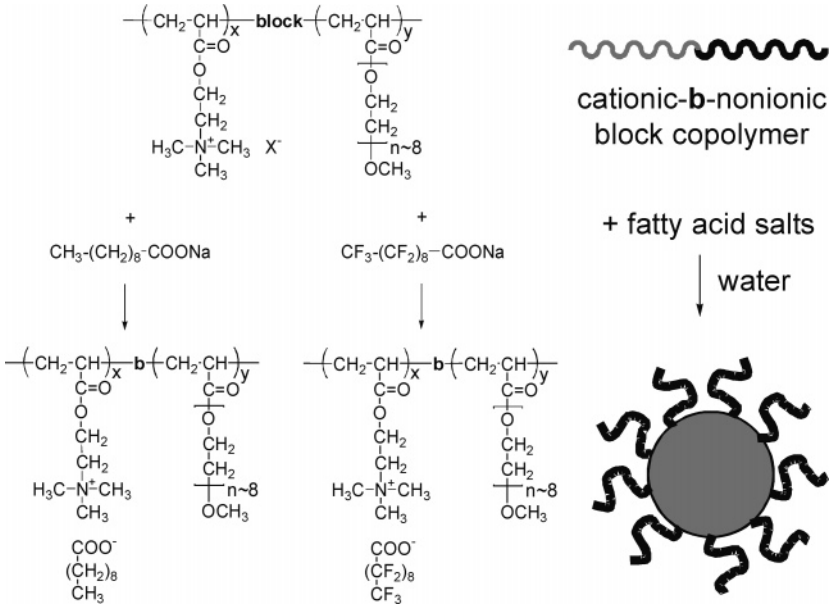


estimation of the content of active RAFT end groups in the polymer. This information is important as the active chain end groups must be preserved as much as possible to enable the efficient synthesis of block copolymers. The molecular data of **polyM1** measured by different methods are given in Table 1. The $M_n$ values calculated by SEC/MALLS ($1.0 \times 10^4$ g mol$^{-1}$, polydispersity = 1.22) and by end group analysis using the naphthalene band at 251 nm ($9.0 \times 10^3$ g mol$^{-1}$) as well as the visible band of the dithioester moiety at 485 nm ($1.2 \times 10^4$ g mol$^{-1}$) are consistent within the precision of the methods, thus indicating a high dithioester end group functionality of the macro RAFT agent.

**V-50** was used as initiator for the blocking of **M2** at 55 °C in water. The SEC traces of the macro RAFT agent **polyM1** and of the final polymer indicate the successful blocking of nonionic macromonomer **M2** on the cationic polyacrylate **polyM1** (Figure 2). The SEC peak of the polymer shifts to lower elution volumes compared to **polyM1** after blocking, while still being monomodal. According to evaluation by MALLS, $M_n$ increases from $1.0 \times 10^4$ to $3.9 \times 10^4$ g mol$^{-1}$, and the polydispersity stays reasonably low with $M_w/M_n = 1.45$. The weight percentages of polymer blocks are analyzed by different methods. Consistently, the copolymer is composed of 24 wt % of **polyM1** block according to microanalysis, and of 25 wt % of **polyM1** block according the integration of the $^1$H NMR spectrum (based on signals "e" and "k", see Figure 3). These values agree well with the increase of $M_n$ deduced by MALLS from the ASEC data (26 wt % of **polyM1**). Additionally, end group analysis was performed by UV−vis spectroscopy for the naphthalene chromophore of the initiating group, as well as for the C═S moiety of the active chain end (Table 1). Interestingly, the resulting $M_n$ values calculated from the different absorbance bands do not agree ($M_n = 3.7 \times 10^4$ g mol$^{-1}$ at $\lambda_{max} = 251$ nm; $M_n = 8.0 \times 10^4$ g mol$^{-1}$ at $\lambda_{max} = 489$ nm). This mismatch strongly suggests that the dithioester end groups are partially lost during the polymerization and purification steps (prolonged reaction and dialysis in water). Since the band at 489 nm depends on the conservation of the dithioester end groups, apparently higher $M_n$ values are calculated with ongoing hydrolysis. In contrast, the UV band at 251 nm results from the initiating naphthyl chromophore which is permanently fixed by a C−C bond. Therefore, the $M_n$ value calculated by this end group should be close to the true value, and match the value derived from MALLS analysis, as is the case. In agreement with this analysis, end group analysis using the absorbance of the UV−vis band at 301 nm, which has contributions from both the naphthalene chromophore as well as the dithiobenzoate group,[8] gives an apparent $M_n$ of $5.7 \times 10^4$ g mol$^{-1}$, in between the two extremes. Thus, end group analysis shows that the copolymer is no more suited for use as macro RAFT agent for further blocking experiments, as many of the active chains ends are hydrolyzed by the procedure chosen. This is an instructive example for the usefulness of labeled RAFT agents and end group analysis in addition to SEC/MALLS, since this information is hard to get otherwise.

Consequently, double hydrophilic block copolymer **polyM1-*block*-M2** with a number-average molar mass $M_n$ of $3.9 \times 10^4$ g mol$^{-1}$ was efficiently produced by aqueous RAFT polymerization. According to combined SEC/$^1$H NMR analysis (cf. Table 1), the cationic block of the copolymer has a molar mass of $1.0 \times 10^4$ g mol$^{-1}$ (number-average degree of polymerization $DP_n = 52$) while the polyethylene oxide based nonionic brushy block has a molar mass of $2.9 \times 10^4$ g mol$^{-1}$ ($DP_n = 66$).

**Nanoparticles Formed by Complexation.** The **polyM1-*block*-M2** was mixed at 60 °C in approximately stoichiometric amounts of the anionic surfactants sodium decanoate and sodium perfluorodecanoate (based on the calculated number of charged groups in the copolymer, the molar ratio of anionic to cationic groups is 1.05:1). The resulting complexes **polyM1-*block*-M2** decanoate (**H−BIC**) and **polyM1-*block*-M2** perfluorodecanoate (**F−BIC**) self-assemble in water to form micellar nanoparticles whose hypothetical structure is presented in Scheme 2. These particles are characterized by a water-swollen poly(ethylene oxide) based corona and a hydrophobic hydrocarbon core for **H−BIC** or a fluorocarbon core for **F−BIC**.

$^1$H NMR spectra of the complexes were compared to the parent copolymer **polyM1-*block*-M2**. The solutions of the particles were lyophilized, and then redissolved in $D_2O$ for the $^1$H NMR measurements (Figure 3). The signal of the C(═O)O−C$H_2$ groups of the **polyM2** block was used as internal reference for the integration of proton signals. In the $^1$H NMR spectrum

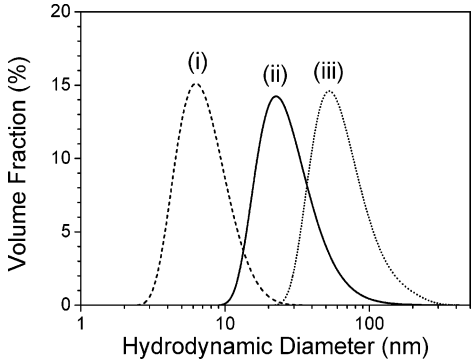


**Figure 4.** DLS analysis of **(i) polyM1-*block*-M2** (dashed line), **(ii)** the **F−BIC** (solid line) and **(iii) H−BIC** (dotted line) in aqueous solution. The maxima are at 6, 22, and 54 nm, respectively.

of **H−BIC**, the protons of cationic block **polyM1** are well visible, as are the signals of decanoate (at about 2.3, 1.2, and 0.8 ppm; Figure 3b), though they are markedly broadened, indicating the formation of hydrophobic aggregates. The decanoate chains and the cationic groups of the complex cannot be completely immobilized in these aggregates, as their signals are still visible in the $^1$H NMR. Presumably, the aggregates groups are plasticized by water. The effect of water as a plasticizer in complexes has been demonstrated earlier by temperature-dependent dynamic mechanical analysis of polyelectrolyte−surfactant complexes in wet and dry state (e.g., the glass transition lowered from 78 °C in dry to 36 °C in wet state).[32]

In contrast, for **F−BIC** prepared with perfluorodecanoate, the proton signals of the copolymer which stems from the protons next to the ester moiety (−C(═O)O−C$H_2$− between 4.1 and 4.6 ppm), and those of the copolymer backbone (between 1.4 and 2.6 ppm) disappear. Moreover, the $^1$H NMR signals of the trimethyl ammonium moiety ($-N^+(CH_3)_3$) are strongly attenuated. The stronger attenuation of the proton signals of **F−BIC** compared to **H−BIC** points to a more reduced mobility of the cationic **polyM1** block after complexation with perfluorodecanoate than with decanoate. This observation is a strong indication for the formation of solid-like hydrophobic domains in the core of the **F−BIC** complexes in water, differing markedly from the behavior of the analogous complex with the hydrocarbon carboxylate **H−BIC**. We explain this difference as a result of the much higher hydrophobicity and higher chain stiffness of perfluorodecanoate compared to decanoate. Note that the critical micelle concentration of a fluorinated surfactant is much lower than that of the corresponding alkyl surfactant, for example, it is $9.0 \times 10^{-4}$ M for potassium perfluorodecanoate and $1.0 \times 10^{-1}$ M for potassium decanoate.[33] Also the Krafft temperature of the fluorinated surfactant is much higher than of its hydrocarbon counterpart.

The aggregation of the block ionomer surfactant complexes in water was studied by dynamic light scattering (DLS). Accordingly, the pure copolymer **polyM1-*block*-M2** has a hydrodynamic diameter of ca. 6 nm and gives only a low scattering signal. This proves that the parent copolymer chains do not self-aggregate. In contrast upon mixing the copolymer with sodium decanoate and sodium perfluorodecanoate, intense scattering nanoparticles (of visible light) are formed (Figure 4) with hydrodynamic diameters of ca. 54 nm (**H−BIC**) and 22 nm (**F−BIC**), respectively. The **H−BIC** and **F−BIC** nanoparticles are stable at room temperature. Note that the Krafft temperature of 39 °C of sodium perfluorodecanoate[34] lies considerably above room temperature, so that it precipitates upon cooling when not complexed with **polyM1-*block*-M2**.

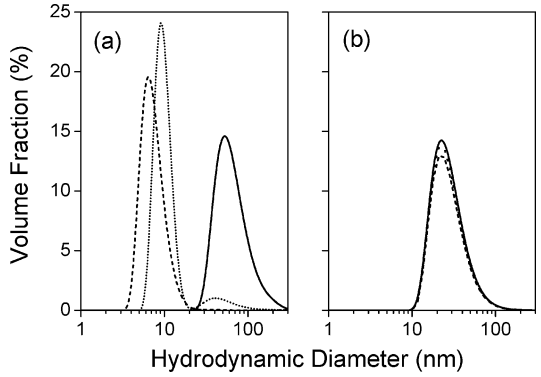


**Figure 5.** DLS analysis of **polyM1-*block*-M2** in water with (a) approximately stoichiometric amounts of sodium decanoate and (b) approximately stoichiometric amounts of sodium perfluorodecanoate. Key: solid lines, sample after preparation (9 mg mL$^{-1}$); dotted lines, sample diluted 3 times; dashed lines, sample after dialysis. The maxima are at 54, 9, and 6 nm in part a and at 22 nm in part b.

The block copolymer and the nanoparticles were also characterized by $\zeta$ potential measurements. The copolymer solution presents fluctuating positive values between +15 and + 40 mV reflecting the absence of aggregates for the polymer alone. The nanoparticles prepared with both surfactants presents $\zeta$-potential values close to zero, namely $-1.1 \pm 1.0$ mV for **H−BIC**, and $-1.3 \pm 1.0$ mV for **F−BIC**. These values of around zero are a strong indication that virtually stoichiometric complexation was achieved; i.e., each cationic monomer group of the polymer chain is complexed with one decanoate molecule.

Because BICs made of single tail surfactants can disintegrate upon dilution,[35] the effect of the dilution on the aggregates was examined. Figure 5 depicts the evolution of the particle size upon dilution followed by DLS. The nanoparticles of **H−BIC**, i.e. made with the hydrocarbon surfactant, preserved their hydrodynamic diameter when the solution was diluted by a factor of 3 from 9 to 3 g mL$^{-1}$. However, further dilution led to their gradual disintegration (Figure 5 a). In contrast, the nanoparticles of **F−BIC**, i.e. made with the fluorocarbon surfactant, were found to be stable, even when dialyzed extensively against large volumes of water (Figure 5b). Changes in the temperature and the salt concentration of the medium may affect the aggregation behavior of BICs, too.[36] Therefore, the stability of sodium perfluorodecanoate particles was examined by DLS in physiological salt solution. No change was observed for the measured hydrodynamic diameter of nanoparticles of **F−BIC** at physiological sodium chloride concentration and body temperature (0.15 M aq NaCl at 37 °C).

**Small-Angle X-ray Scattering.** Further structure information on the particles was obtained by small-angle X-ray scattering. The fluorinated nanoparticles produced a high scattering intensity (Figure 6) while the intensity of the alkylated nanoparticles is low (not shown). Such was observed earlier for nanoparticles formed by complexes of poly(*N,N′*-dimethylammonium-*alt*-*N*-phenylmaleamic carboxylate) and the sodium salt of (i) dodecanoic acid and (ii) perfluorododecanoic acid.[28] The reason for the large difference in scattering intensity is the much higher electron density of the fluorinated nanoparticles compared with the alkylated particles.[27] Taking into account that the small-angle scattering is proportional to the square of the electron density difference between the particles and their surroundings (water), the scattering intensity of the fluorinated particles is expected to be at least an order of magnitude higher than that of their alkylated analogues. On the basis of the present data, we can therefore only evaluate the SAXS of the fluorinated nanoparticles (in a concentration range of 3−30 g L$^{-1}$).

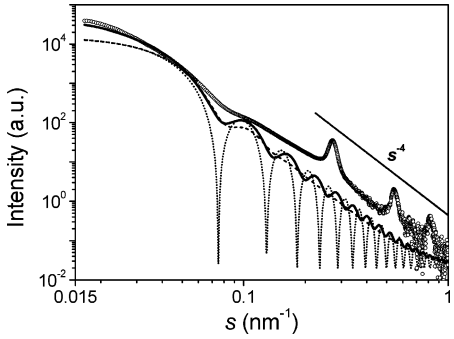


**Figure 6.** Small-angle X-ray scattering of **F−BIC** nanoparticles (symbols) and the scattering curves of monodisperse spheres ($R = 9.5$ nm, dotted line), polydisperse spheres ($R = 9.5$ nm, $\sigma = 0.14$, dashed line) and prolate ellipsoids (short semiaxis = 8.5 nm, long semiaxis = 23.8 nm, $\epsilon = 2.8$ nm, solid line). The **F−BIC** concentration was 9 g L$^{-1}$.

It can be seen in Figure 6 that the SAXS curve of **F−BIC** shows the typical scattering profile produced by noninteracting particles for scattering vectors in the range of $s = 0.016$ to about 0.2 nm$^{-1}$. However, equidistant reflections are found at higher $s$ values with maxima at 0.274, 0.544, and 0.820 nm$^{-1}$, corresponding to a lamellar nanostructure with a long period of $d = 3.65$ nm. Furthermore, at high $s$ values, the overall scattering intensity decreases proportional to $s^{-4}$ as indicated by a straight line in Figure 6. This $s^{-4}$ scaling is in accordance to Porod's law, which is only observed when sharp transitions in the electron density are present. A gradual transition in the density between the core of the nanoparticles and their surrounding shell, e.g., such as quantitatively described by Förster for core−shell structures of polymeric micelles,[37,38] can be excluded for **F−BIC**. Small deviations from a sharp boundary result in a significant deviation from Porod's law.[39,40] We can therefore conclude that the transition (in terms of electron density) between the cores and their surroundings is of the order of 1−2 atomic distances. At first this observation seems to be in contradiction to our assumption of a core−shell particle structure. However, when using X-rays to probe the structure, we cannot expect to see the shell. The reason is the following: A shell of water-swollen PEO chains has an electron-density close to that of pure water when compared with the fluorinated core. As a consequence, the presumed shell, which sterically stabilizes the particles in water and prevents their aggregation, is here practically invisible with SAXS. Note that steric stabilization by PEO chains is assumed because the zero $\zeta$ potential value recorded indicate that significant electrostatic stabilization contributions must be excluded. The consideration of only two phases is sufficient in our case, because the scattering power is a function of the square of the contrast between two phases (core and its surrounding of water-swollen PEO shell). We measured a density of 2.035 g cm$^3$ for **F−BIC**. This value is similar to that of amorphous polytetrafluoroethylene[41] (density $\approx$ 2 g mol$^{-1}$). It is higher than reported earlier for polyelectrolyte-dressed perfluorododecanoate micelles (1.442−1.754 g cm$^3$)[27] and polyelectrolyte-perfluorodecanoate complexes as bulk materials (1.44−1.87 g cm$^{-3}$).[42] The high density of **F−BIC** proves that the perfluorodecanoate molecules must be tightly packed in the cores. Accordingly, the scattering from the small contrast between the second phase (water-swollen PEO shell) and the third phase (water) is negligible. A detailed argumentation for cases in which three phases instead of two have to be considered is given elsewhere.[43,44]

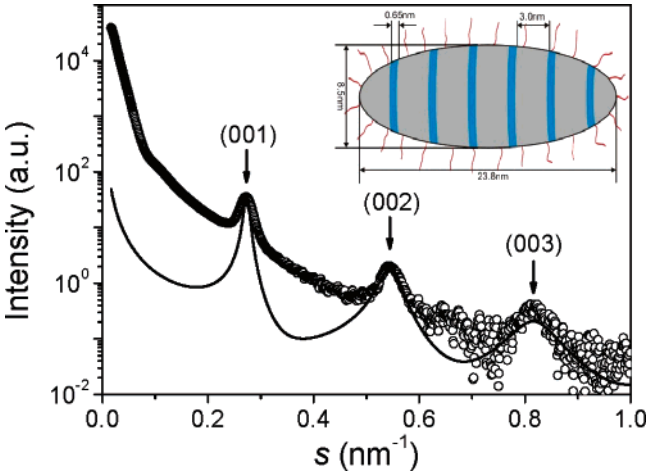


**Figure 7.** Small-angle X-ray scattering curve of **F−BIC** (symbols). Arrows indicate the scattering maxima at 0.274, 0.544, and 0.820 nm$^{-1}$. The solid line corresponds to a stack of lamellae with a periodicity of $L = 3.65$ nm and with thicknesses $d_1 = 3.00$ nm and $d_2 = 0.65$ nm of the lamellae rich in perfluoroalkyl groups and ionic groups, respectively ($\sigma_1 = \sigma_2 = 0.2$ nm). The inset shows a sketch of the core structure of **F−BIC** nanoparticles.

**Prolate Ellipsoidal-Shaped Nanoparticles.** The simultaneous appearance of particle scattering and Bragg peaks is rare. It has been observed for gels of perfluorinated liquids formed with *N*-alkylated perfluoroalkanamides.[45] Therein the organic gel-forming molecules (gelators) aggregate into lamellae within a network of fibrils. In such a system the solution viscosity and the scattering pattern strongly depend on concentration. In contrast to such systems, the viscosity of the **F−BIC** solution is low. We quantified the viscosity from a Huggins plot resulting in $[\eta] = 18.11$ cm$^3$ g$^{-1}$ and a Huggins constant of $k_H = 2.59$. Further, the shape of the scattering curve is independent of the concentration, which is consistent with our results from DLS and $\zeta$ potential measurements.

For these reasons, we have to conclude that the scattering of **F−BIC** results from noninteracting individual particles; i.e., the structure factor is unity and the scattering is given by the form factor $P(s)$ alone. We assume a spherical shape of the particles as a first step to estimate the particle size. In the case of monodisperse spheres the scattering amplitude is

$$\Phi(s, R) = \frac{3[\sin(2\pi sR) - 2\pi sR\cos(2\pi sR)]}{(2\pi sR)^3} \qquad (1)$$

The form factor is equal to the modulus of the square of the scattering amplitude $P_{mono}(s, R) = |\Phi(s, R)|^2$. Polydispersity of spherical particles is taken into account by averaging aver a Schulz−Zimm distribution[38]

$$P_{poly}(s) = \int_0^\infty P_{mono}(s, R)h(R)\,dR \qquad (2)$$

with

$$h(R) = \frac{(z+1)^{z+1}R^z}{\langle R\rangle^{z+1}\Gamma(z+1)}\exp\left[-(z+1)\frac{R}{\langle R\rangle}\right] \qquad (3)$$

Therein we have the average radius $\langle R\rangle$ and the relative standard deviation $\sigma = (z+1)^{-1/2}$.

It can be seen in Figure 6 that the scattering of monodisperse spheres with a radius of 9.5 nm is suitable as a first estimate for the particle sizes (dotted line). The position of the first minimum, in particular, is reproduced. The general shape of

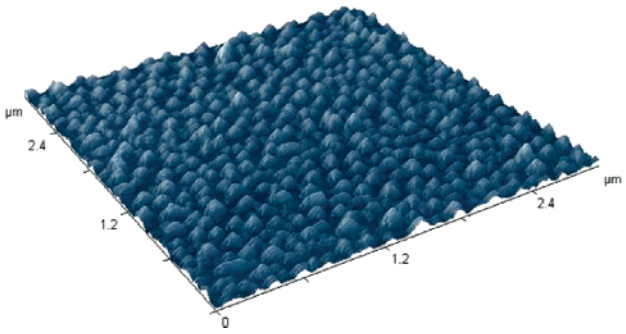


**Figure 8.** Atomic force microscope image with the height profile of **F−BIC** nanoparticles dried from aqueous solution on a mica surface. The average height of the particles is about 9 nm.

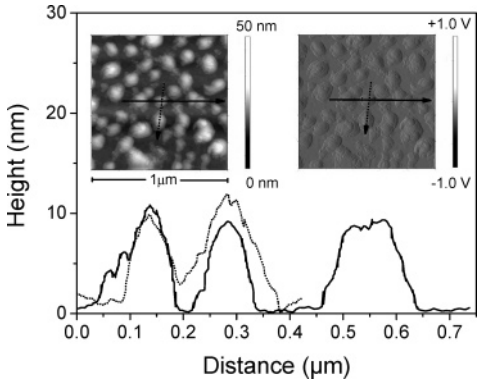


**Figure 9.** AFM sections of height images of the **F−BIC** nanoparticles on mica with a height of about 9 nm. The insets are a topography image (left) and phase contrast image (right). The arrows indicate sections along the horizontal (solid line) and vertical direction (dotted line). In the main figure, the corresponding height profiles of these sections display three (solid line) and two particles (dashed line), respectively.

the experimental curve (damping of the oscillation) is better reproduced when taking the same radius, but with a polydisperse size distribution according to eq 2 with a relative standard deviation of $\sigma = 0.14$ (Figure 6, dashed line).

It can be seen there that the shape of the experimental scattering curve at small $s$ is steeper than can produced by a spherical object only. This is indicative of prolate (elongated) ellipsoids. The form factor of elliptical particles with the semiaxes $R$, $R$, and $\epsilon R$, useful for the description of elliptical cores of triblock copolymer micelles,[46] is given by[47]

$$P_{\text{ellipse}}(s, R, \epsilon) = \int_0^{\pi/2} \Phi^2[s, r(R, \epsilon, \alpha)]\sin \mathrm{d}\alpha \qquad (4)$$

where $r(R, \epsilon, \alpha) = R(\sin^2 \alpha + \epsilon^2 \cos^2 \alpha)^{1/2}$. The $\epsilon > 1$ for prolate ellipsoids and $\epsilon < 1$ for oblate ellipsoids. When using eq 4 we found that the scattering of prolate ellipsoids with two short semiaxes of $R = 8.5$ nm and a long semiaxis of $\epsilon R = 23.8$ nm ($\epsilon = 2.8$) reproduces the experimental data well (see solid line in Figure 6). It is obvious that the description of the data can be further improved when polydispersity is introduced. A distribution of $R$ with a small $\sigma$ of about 10% will already dampen the oscillations of the scattering curve. To the best of our knowledge there is currently no useful expression that describes the scattering of polydisperse ellipsoids. Therefore, we take the polydispersity of 14% derived from the polydisperse sphere model $R$ as an approximation. The scattering intensity at very small angles can be described by Guinier's approximation, which gives the radius of gyration, $R_g$, of nanoparticles: $\ln[I(s)] = \ln[I(s = 0)] - 4/3\pi^2 R_g^2 s^2$. According to this we determined $R_g = 11.7$ nm from a Guinier plot (not shown). The

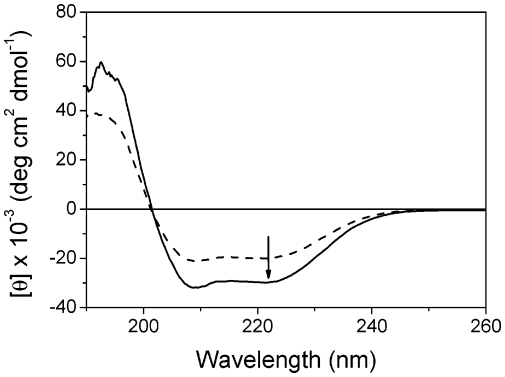


**Figure 10.** Circular dichroism of HSA without (dashed line) and with **F−BIC** nanoparticles (solid line). The arrow indicates the decrease in ellipticity at 222 nm due to incubation with the nanoparticles.

$R_g$ can be determined independent of the particle shape from SAXS but it is only valid if the particles are noninteracting. Interacting values produce much higher (apparent) values. The theoretical radius of gyration for our prolate ellipsoid nanoparticles, $R_{g,\text{ellipsoid}}^2 = 1/5(2R^2 + (\epsilon R)^2)$, is $R_g = 11.9$ nm. This is in accordance with our measured value and confirms the assumption of a prolate ellipsoid structure.

**Lamellar Structured Cores.** Our analysis of the lamellar structured core of the particles is based on the approach developed by Ruland et al.[40] This was successfully applied for the analysis of extended lamellar nanocomposites.[48] We assume that the core of **F−BIC** can be described by a stack of lamellae with a periodicity of $L$ formed by alternating layers of type 1 and type 2, with average thicknesses $d_1$ and $d_2$. (enriched in perfluoroalkyl chains and in ionic groups, respectively). The thicknesses have the standard deviations $\sigma_1$ and $\sigma_2$. For randomly oriented stacks given by freely diffusing nanoparticles one obtains

$$I(s) \propto \frac{1}{s^2} \mathrm{Re}\left[\frac{(1 - H_1(s))(1 - H_2(s))}{(1 - H_1(s)H_2(s))}\right] \qquad (5)$$

with

$$H_i(s) = \exp(2\pi i d_i - 2\pi^2 \sigma_i^2 s^2) \qquad (6)$$

Applying eq 5 to interpret the SAXS pattern from **F−BIC**, we found that peak positions (sensitive to $L$), relative intensities (sensitive to the ratio of $d_1$ to $d_2$) and peak widths (sensitive to $\sigma_1$ and $\sigma_2$) are well reproduced. The solid line in Figure 7 corresponds to a stack of lamellae with thicknesses $d_1 = 3.00$ nm and $d_2 = 0.65$ nm and a periodicity $L = d_1 + d_2 = 3.65$ nm. The standard deviations are $\sigma_1 = \sigma_2 = 0.2$ nm. We assign $d_1$ to the nonionic lamellae which are enriched in the perfluorinated alkyl chains (in extended conformation) and $d_2$ to the lamellae enriched in the polyelectrolyte chains plus the carboxylic head groups. The values determined for $d_1$ and $d_2$ are typical for polyelectrolyte−surfactant complexes with a lamellar solid-state structure in bulk materials and thin films.[1] In principle, structure characteristics of stack height and width can be also derived, but this overstresses the model. A sketch that summarizes our final structure model of the **F−BIC** nanoparticles is given in the inset of Figure 7.

**Visualization of the Nanoparticles.** The dimensions of the **F−BIC** nanoparticles are suited for visualization by atomic force microscopy (AFM). The AFM in tapping mode allows nondestructive imaging of the surface of soft polymer samples and was recently successfully used to characterize core(hard)−shell-

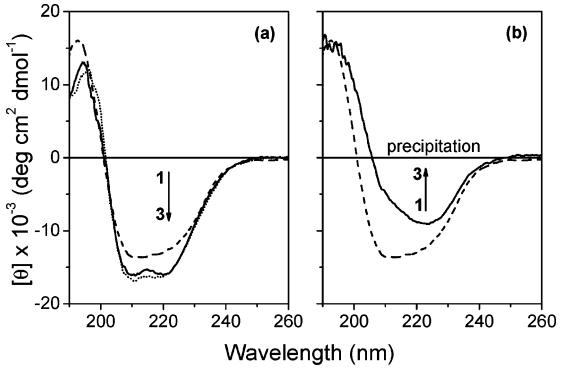


**Figure 11.** Circular dichroism of fibrinogen in buffer ($K_2HPO_4/KH_2PO_4$) at pH 7: (a) in contact with **F−BIC** nanoparticles, and (b) in contact with noncomplexed **polyM1-*block*-M2**. Key: dashed lines (----), native state before incubation; solid lines (——), state after 10 min of incubation; dotted line (·····), state after 24 h of incubation. In the case of added **polyM1-*block*-M2**, the fibrinogen was precipitated after 24 h of incubation.

(soft) morphology of hockey puck micelles formed by rod−coil block copolymers.[49] For visualization of the nanoparticles, one drop of the **F−BIC** dispersion was cast onto freshly cleaved mica, the negatively charged surface of which offers good adhesion for hydrophilic polymers like PEO. After evaporation of the water, the sample was examined by AFM. A height profile of a region of 2.6 $\mu$m × 2.6 $\mu$m in size is shown in Figure 8 where spherical or slightly oval-shaped particles are densely packed, displaying relative uniform particle heights and lateral dimensions of ≤100 nm. Obviously individual particles remain discrete even after drying. Only some aggregates where two or three particles seem to be merged on the mica surface can be observed. A height profile and a phase image with a higher magnification of the particles are displayed in the insets of Figure 9. Representative height profiles through two nanoparticles and two nanoparticles plus an aggregate of two particles are shown in Figure 9 (dotted and solid line, respectively). It can be seen clearly that the size of dried **F−BIC** nanoparticles is 9 nm in height and about 100 nm in width. Taking into account that the particles flatten strongly due to the drying process the overall size of the nanoparticle as determined from AFM in its dry state and from DLS in solution are consistent. Interestingly the shape anisotropy of the nanoparticle core is much more pronounced than that of the overall nanoparticle. This is not necessarily self-contradictory as has been reported for hockey puck micelles.[49] Most likely the stretching of the neutral block **polyM2** at the rod−coil boundary (i. e. boundary between complexed **polyM1** and **polyM2**), results in stretched linear **polyM2** blocks in the vicinity of the core. The **polyM2** block becomes more coiled with increasing distance from the core and canceling out the axial ratio anisotropy of the core itself to some degree.

**Increase of the α-Helix Content of HSA and Fibrinogen.** Understanding and controlling protein adsorption is decisive for designing biocompatible nanoparticles. In particular, for any potential in vivo application, the interactions of nanoparticles with natural proteins are crucial, as they may denaturate the natural proteins. In this context the effects of $CF_3$ groups on the human serum albumin (HSA) secondary structure have been investigated when in contact with surfaces of polymer fluorosurfactant complexes.[50] In general the secondary structure of HSA was maintained, but in some cases the α-helix content increased. For one complex containing perfluorooctanoic acid, for example, it was possible to achieve 76% helix for adsorbed HSA, a value ∼10% above the native one. Therefore, we wondered whether the stable **F−BIC** nanoparticles might influence also the secondary structure of HSA. In order to find out whether **F−BIC** change the secondary structure of proteins, preliminary tests were carried out with HSA and fibrinogen, two major blood plasma proteins. First, the particles were mixed with HSA in $KH_2PO_4/K_2HPO_4$ buffer solution, and the circular dichroism of this mixture was compared with that of HSA in the same buffer solution. As is seen in Figure 10, the spectra display two minima, one at 208 nm and the other one at 222 nm, characteristic of α-helical structure. These minima are more pronounced in the presence of the **F−BIC** indicating that the amount of α-helix in HSA was increased. The crystal structure of HSA is well characterized[51] and has 28 α-helical segments which amount to 67%. Comparing the measured ellipticity values at 222 nm with and without **F−BIC** we found that the α-helix content increases by incubation with **F−BIC** to a constant value within a few minutes. The change of the mean residue ellipticity at 222 nm, $[\theta]_{222}$, varies linearly with the α-helix content of a protein,[52] which allows to easily estimate the change in the α-helical content of a protein from the $[\theta]_{222}$. When taking an α-helical content of 67% for HAS in its native state then the α-helix content increases to 100% by the incubation with **F−BIC** within minutes. The formula of Greenfield and Fasman[53] is also very commonly used to estimate the α-helix content of a protein:[54]

$$\alpha(\%) = \frac{-[\theta]_{222} - 4000}{33000 - 4000} \times 100 \qquad (7)$$

Using eq 7, we determined an α-helix content of about 55% for HSA without and 89% with incubation of **F−BIC**. Messina calculated a similar value for pure HSA in buffer when using the eq 7 (53.1% α-helix).[54] Despite the fact that the absolute values of the α-helix content have to be discussed controversially, we conclude that **F−BIC** strongly increases the amount of α-helix in HSA.

The second protein, fibrinogen, has frequently been investigated in biomaterial interaction because of its relevance to thrombotic interactions with blood-contacting materials and because of its distinctive shape. While HSA is a globular protein, fibrinogen is a flexible elongated molecule (dimensions are 47 × 4.5 × 4.5 $nm^3$). It highly adsorbs to surfaces with very low surface mobility.[55]

Circular dichroism spectra of fibrinogen were measured under the same condition as for HSA. It can be seen in Figure 11a (dashed and solid line) that the CD spectrum of fibrinogen changes within 10 min of incubation with **F−BIC**. After incubation it display the shape typical for a high α-helix content. It can be seen also that the further changes in the spectrum within the next 24 h are small (Figure 11a, dotted line). No aggregation was observed. For comparison, after 10 min of incubation with the noncomplexed **polyM1-*block*-M2** (Figure 11, solid line in part b), the ellipticity around 222 nm increased. Accordingly the content of α-helix in fibrinogen had decreased by incubation with the pure polymer. Finally the fibrinogen precipitated and no CD signal was obtained after 24 h. Similar results were obtained when using **H−BIC**.

For quantification of the α-helix content in fibrinogen,[56] we used eq 7 resulting in 29% of α-helix for the pure fibrinogen which is comparable to the value reported in the literature (e.g., Chen et al.[57] determined 35.4%). After 10 min of incubation we calculated α-helix contents of 68% with **F−BIC** and 17% with **polyM1-*block*-M2**. This value increased slightly after 24 h of incubation with **F−BIC** to 70% while no α-helix content could be detected after incubation with the pure polymer due

to precipitation. Because of fibrinogen is known for its quick adsorption to foreign materials and due to its vital role in clot formation it is interesting that it behaves very unexpectedly by forming a secondary structure highly enriched in α-helix when in contact with **F−BIC**. In the control experiment with pure **polyM1-*block*-M2**, fibrinogen looses its ordered structure and precipitated as expected. This proves that the α-helix formation is a distinct property of the **F−BIC** nanoparticles and not of the block copolymer. A control experiment with the pure perfluorodecanoate was not possible because it is not sufficiently soluble below 40 °C. Earlier studies have shown that the adsorption of fibrinogen to biomedical polyurethanes and perfluorinated polymers is also accompanied by strong conformational changes that highly depends on the chemical properties of the surface.[58] To the best of our knowledge the strong α-helix inducing property of **F−BIC**, at least on the structure of fibrinogen, is unique. A comparative study to other strong α-helix forming agents like fluoro alcohols (trifluoroethanol and hexafluoro-2-propanol)[59] may help to understand the mechanisms of protein folding.

## Conclusion

The **F−BIC** nanoparticles exemplify the potential of functional/complex polymers which can be synthesized via RAFT in water. For any biomedical application of polymer-based nanoparticles, the structure of such a polymer should be well-defined, and this can be achieved via RAFT polymerization in water. Importantly, all the steps for the preparation of nanoparticles including polymer synthesis were carried out in water. Therefore, the risk of having residual organic solvents in hydrophobic core of particles, which may cause serious problems for any in vivo application, can be excluded in this strategy, as well.

**Acknowledgment.** The help of S. Bruzzano and Ch. Wieland (both Fraunhofer IAP) for MALLS−SEC is gratefully acknowledged. We thank F. Emmerling (BAM) for synchrotron SAXS measurement. The work was financially supported by the Fonds der Chemischen Industrie and the Federal Institute for Materials Research and Testing (BAM).

## References and Notes

(1) Thünemann, A. F.; Müller, M.; Dautzenberg, H.; Joanny, J. F. O.; Lowne, H. Polyelectrolyte complexes. In *Polyelectrolytes with Defined Molecular Architecture II*; Schmidt, M. Ed.; Advances in Polymer Science 166; Springer: Berlin, 2004; pp 113−171.
(2) Thünemann, A. F.; Beyermann, J.; Kukula, H. *Macromolecules* **2000**, *33*, 5906−5911.
(3) Harada, A.; Kataoka, K. *Langmuir* **1999**, *15*, 4208−4212.
(4) Kabanov, A. V.; Bronich, T. K.; Kabanov, V. A.; Yu, K.; Eisenberg, A. *Macromolecules* **1996**, *29*, 6797−6802.
(5) Ruokolainen, J.; Torkkeli, M.; Serimaa, R.; Vahvaselka, S.; Saariaho, M.; tenBrinke, G.; Ikkala, O. *Macromolecules* **1996**, *29*, 6621−6628.
(6) McCormick, C. L.; Lowe, A. B. *Acc. Chem. Res.* **2004**, *37*, 312−325.
(7) Baussard, J. F.; Habib-Jiwan, J. L.; Laschewsky, A.; Mertoglu, M.; Storsberg, J. *Polymer* **2004**, *45*, 3615−3626.
(8) Mertoglu, M.; Laschewsky, A.; Skrabania, K.; Wieland, C. *Macromolecules* **2005**, *38*, 3601−3614.
(9) Garnier, S.; Laschewsky, A. *Macromolecules* **2005**, *38*, 7580−7592.
(10) Mertoglu, M.; Garnier, S.; Laschewsky, A.; Skrabania, K.; Storsberg, J. *Polymer* **2005**, *46*, 7726−7740.
(11) Kataoka, K.; Matsumoto, T.; Yokoyama, M.; Okano, T.; Sakurai, Y.; Fukushima, S.; Okamoto, K.; Kwon, G. S. *J. Contr. Rel.* **2000**, *64*, 143−153.
(12) Zhang, X. C.; Jackson, J. K.; Burt, H. M. *Int. J. Pharm.* **1996**, 132, 195−206.
(13) Bronstein, L. H.; Sidorov, S. N.; Valetsky, P. M.; Hartmann, J.; Cölfen, H.; Antonietti, M. *Langmuir* **1999**, *15*, 6256−6262.
(14) Thünemann, A. F.; Kubowicz, S.; Burger, C.; Watson, M. D.; Tchebotareva, N.; Müllen, K. *J. Am. Chem. Soc.* **2003**, *125*, 352−356.
(15) Nagarajan, R.; Barry, M.; Ruckenstein, E. *Langmuir* **1986**, *2*, 210−215.
(16) Hurter, P. N.; Hatton, T. A. *Langmuir* **1992**, *8*, 1291−1299.
(17) Spatz, J. P.; Sheiko, S.; Möller, M. *Macromolecules* **1996**, *29*, 3220−3226.
(18) Webber, S. E. *J. Phys. Chem. B* **1998**, *102*, 2618−2626.
(19) Garnier, S.; Laschewsky, A. *Langmuir* **2006**, *22*, 4044−4053.
(20) Dong, C. M.; Chaikof, E. L. *Colloid Polym. Sci.* **2005**, *283*, 1366−1370.
(21) Garnier, S.; Laschewsky, A. *Colloid Polym. Sci.* **2006**, *284*, 1243−1254.
(22) Street, G.; Illsley, D.; Holder, S. J. *J. Polym. Sci., Part A: Polym. Chem.* **2005**, 43, 1129−1143.
(23) Ishizone, T.; Han, S.; Hagiwara, M.; Yokoyama, H. *Macromolecules* **2006**, 39, 962−970.
(24) Hua, F. J.; Jiang, X. G.; Zhao, B. *Macromolecules* **2006**, *39*, 3476−3479.
(25) Du, J. Z.; Chen, D. P.; Wang, Y. C.; Xiao, C. S.; Lu, Y. J.; Wang, J.; Zhang, G. Z. *Biomacromolecules* **2006**, *7*, 1898−1903.
(26) Bhadra, D.; Bhadra, S.; Jain, P.; Jain, N. K. *Pharmazie* **2002**, *57*, 5−29.
(27) Thünemann, A. F.; Sander, K.; Jaeger, W.; Dimova, R. *Langmuir* **2002**, *18*, 5099−5105.
(28) Rocha, S.; Thünemann, A. F.; Pereira, M. C.; Coelho, M. A. N.; Möhwald, H.; Brezesinski, G. *Chembiochem* **2005**, *6*, 280−283.
(29) Laschewsky, A.; Garnier, S.; Kristen, J.; Mertoglu, M.; Skrabania, K.; Lutz, J.-F. *Polym. Mater. Sci. Eng.* **2006**, *94*, 307−308.
(30) Moad, G.; Mayadunne, R. T. A.; Rizzardo, E.; Skidmore, M.; Thang, S. H. *Macromol. Symp.* **2003**, *192*, 1−12.
(31) Albertin, L.; Stenzel, M. H.; Barner-Kowollik, C.; Davis, T. P. *Polymer* **2006**, *47*, 1011−1019.
(32) Thünemann, A. F.; Lochhaas, K. H. *Langmuir* **1999**, *15*, 4867−4874.
(33) Hoffmann, H.; Wurtz, J. *J. Mol. Liq.* **1997**, *72*, 191−230.
(34) Ikawa, Y.; Tsuru, S.; Murata, Y.; Okawauchi, M.; Shigematsu, M.; Sugihara, G. *J. Sol. Chem.* **1988**, *17*, 125−137.
(35) Bronich, T. K.; Ming, O. Y.; Kabanov, V. A.; Eisenberg, A.; Szoka, F. C.; Kabanov, A. V. *J. Am. Chem. Soc.* **2002**, *124*, 11872−11873.
(36) Solomatin, S. V.; Bronich, T. K.; Eisenberg, A.; Kabanov, V. A.; Kabanov, A. V. *Langmuir* **2004**, *20*, 2066−2068.
(37) Förster, S.; Burger, C. *Macromolecules* **1998**, *31*, 879−891.
(38) Förster, S.; Hermsdorf, N.; Bottcher, C.; Lindner, P. *Macromolecules* **2002**, *35*, 4096−4105.
(39) Siemann, U.; Ruland, W. *Colloid Polym. Sci.* **1982**, *260*, 999−1010.
(40) Wolff, T.; Burger, C.; Ruland, W. *Macromolecules* **1994**, *27*, 3301−3309.
(41) van Krevelen, D. W. *Properties of Polymers*; Elsevier: Amsterdam, 1990.
(42) Thünemann, A. F.; Lochhaas, K. H. *Langmuir* **1998**, *14*, 4898−4903.
(43) Janosi, A. *Monatsh. Chem.* **1983**, *114*, 377−383.
(44) Janosi, A. *Z. Phys. B: Condens. Matter* **1986**, *63*, 383−387.
(45) George, M.; Snyder, S. L.; Terech, P.; Weiss, R. G. *Langmuir* **2005**, *21*, 9970−9977.
(46) Lodge, T. P.; Xu, X.; Ryu, C. Y.; Hamley, I. W.; Fairclough, J. P. A.; Ryan, A. J.; Pedersen, J. S. *Macromolecules* **1996**, *29*, 5955−5964.
(47) Guinier, A. *X-Ray Diffraction in Crystals, Imperfect Crystals, and Amorphous Bodies*; W. H. Freemann: San Francisco, CA, 1963; p 326.
(48) Garnweitner, G.; Smarsly, B.; Assink, R.; Ruland, W.; Bond, E.; Brinker, C. J. *Am. Chem. Soc.* **2003**, *125*, 5626−5627.
(49) Schleuss, T. W.; Abbel, R.; Gross, M.; Schollmeyer, D.; Frey, H.; Maskos, M.; Berger, R.; Kilbinger, A. F. M. *Angew. Chem., Int. Ed.* **2006**, *45*, 2969−2975.
(50) Coelho, M. A. N.; Vieira, E. P.; Motschmann, H.; Möhwald, H.; Thünemann, A. F. *Langmuir* **2003**, *19*, 7544−7550.
(51) He, X. M.; Carter, D. C. *Nature (London)* **1992**, *358*, 209−215.
(52) Chen, Y. H.; Yang, J. T.; Martinez, H. M. *Biochemistry* **1972**, *11*, 4120−4131.
(53) Greenfield, N.; Fasman, G. D. *Biochemistry* **1969**, *8*, 4108−4116.
(54) Messina, P.; Prieto, G.; Dodero, V.; Ruso, J. M.; Schulz, P.; Sarmiento, F. *Biopolymers* **2005**, *79*, 300−309.
(55) Toscano, A.; Santore, M. M. *Langmuir* **2006**, *22*, 2588−2597.
(56) Weisel, J. W.; Stauffacher, C. V.; Bullitt, E.; Cohen, C. *Science* **1985**, *230*, 1388−1391.
(57) Chen, Y. L.; Zhang, X. F.; Gong, Y. D.; Zhao, N. M.; Zeng, T. Y.; Song, X. Q. *J. Colloid Interface Sci.* **1999**, *214*, 38−45.
(58) Clarke, M. L.; Wang, J.; Chen, Z. *Phys. Chem. B* **2005**, *109*, 22027−22035.
(59) Kumar, Y.; Tayyab, S.; Muzammil, S. *Arch. Biochem. Biophys.* **2004**, *426*, 3−10.

MA061573K